

File ID 144796
Filename 8: Type I X-ray bursts, burst oscillations and kHz quasi-periodic oscillations
in the neutron star system IGR J17191-2821

SOURCE (OR PART OF THE FOLLOWING SOURCE):

Type Dissertation
Title Accretion states and thermonuclear bursts in neutron star X-ray binaries
Author M. Linares Alegret
Faculty Faculty of Science
Year 2009
Pages vi, 194

FULL BIBLIOGRAPHIC DETAILS:

<http://dare.uva.nl/record/314294>

Copyright

It is not permitted to download or to forward/distribute the text or part of it without the consent of the author(s) and/or copyright holder(s), other than for strictly personal, individual use.

8 Type I X-ray bursts, burst oscillations and kHz quasi-periodic oscillations in the neutron star system IGR J17191-2821

Diego Altamirano, Manuel Linares, Alessandro Patruno, Nathalie Degenaar,
Rudy Wijnands, Marc Klein-Wolt, Michiel van der Klis, Craig B.
Markwardt, Jean Swank

Monthly Notices of the Royal Astronomical Society, 2009, submitted

Abstract

We present a detailed study of the X-ray energy and power spectral properties of the neutron star transient IGR J17191–2821. We discovered four instances of simultaneous pairs of kilohertz quasi-periodic oscillations (kHz QPOs) and five thermonuclear type-I X-ray bursts. We found that the frequency difference between kHz QPOs is between 315 Hz and 362 Hz. We also detected burst oscillations at ~ 294 Hz during three of the X-ray bursts. Finally, we report on a faint and short outburst precursor, which occurred about two months before the main outburst. Our results on the broadband spectral and variability properties allow us to firmly establish the atoll source nature of IGR J17191–2821.

8.1 Introduction

Neutron star low-mass X-ray binaries (NS-LMXBs) have been extensively observed with the *Rossi X-ray Timing Explorer* (RXTE) during the last 13 years. These observations have led to important discoveries, such as persistent and intermittent pulsations in accretion-powered millisecond X-ray pulsars, nearly coherent oscillations during X-ray bursts and strong quasi-periodic variability on millisecond time-scales (the so called kilohertz quasi-periodic oscillations; kHz QPOs).

In neutron star LMXBs, the kHz QPOs are relatively narrow peaks in the power spectrum. They appear (sometimes) in pairs, are usually called L_u and L_ℓ (u and ℓ stand for upper and lower, respectively, based on their frequency). These QPOs are thought to reflect motion of matter around the neutron star at the inner edge of the accretion disk (see, e.g. Miller et al. 1998). While it is often assumed that at least one of them reflects the Keplerian frequency at the inner edge of the accretion disk (see e.g. review by van der Klis 2006), models have to still satisfactorily explain the presence and characteristics of both of them. Up to date, kHz QPOs with similar characteristics have been detected in about 30 neutron star sources.

Direct detection of coherent or nearly coherent pulsations is the only available method to measure the neutron star spin period in LMXBs. Ten NS-LMXBs out of more than 100 known (Liu et al. 2007) have shown coherent millisecond pulsations in their persistent emission; these systems are known as accretion-powered millisecond X-ray pulsars (AMXPs; see Wijnands 2005, for a review of the first six AMXPs discovered; for the last four see Kaaret et al. 2006, Krimm et al. 2007b, Casella et al. 2008 and Altamirano et al. 2008a). Sixteen sources to date (including the one presented in this paper) have shown nearly coherent millisecond oscillations during thermonuclear Type-I X-ray bursts (Watts et al. 2008a, 2009b). As the X-ray burst evolves, the oscillation frequency typically increases by a few Hz, approaching an asymptotic value (ν_{BO}) which is stable for a given source from burst to burst. This asymptotic frequency is thought to trace within a few Hz the spin frequency of the neutron star (Strohmayer et al. 1996b). In some AMXPs ν_{BO} is more stable in individual bursts. The AMXPs SAX J1808-3658 (Chakrabarty et al. 2003), XTE J1814-338 (Strohmayer et al. 2003), Aql X-1 (Casella et al. 2008) and most recently HETE J1900.1-2455 (Watts et al. 2009b) have all shown $\nu_s \simeq \nu_{BO}$, strongly supporting this connection between ν_{BO} and ν_s .

Since the discovery of burst oscillations and two simultaneous kHz QPOs in neutron star LMXBs, it was suggested that there was a relation between the neutron star spin frequency, ν_s , and the kHz QPO frequency difference

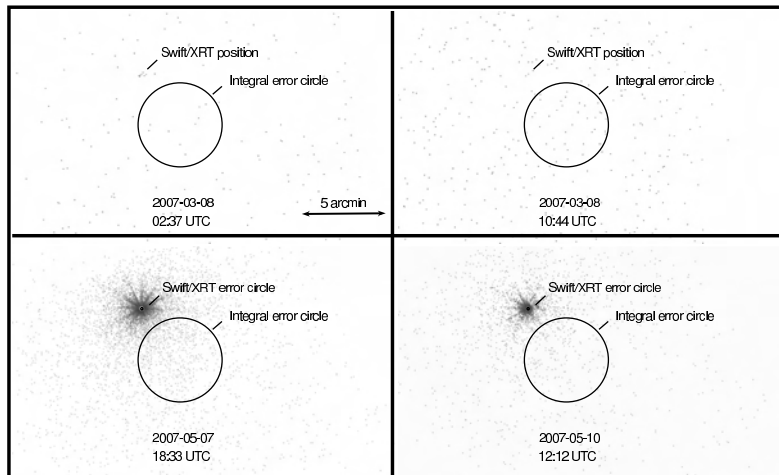


Figure 8.1: Swift/XRT images of IGR J17191–2821. The INTEGRAL error circle for the position is plotted in each case. The scale is the same for all panels. The source showed an outburst precursor or flare on March 8th, as it was detected at 02:37 UT (upper-left panel) and undetected at 10:44 UT (upper-right panel). The source was in outburst in May (lower panels). See Section 8.3.1 for more details.

$\Delta\nu = \nu_u - \nu_\ell$. Although the frequency of the QPOs was found to vary ($150 \lesssim \nu_\ell \lesssim 900$ Hz and $350 \lesssim \nu_u \lesssim 1200$ Hz), at first instance $\Delta\nu$ was consistent with being constant¹ and equal to the asymptotic burst oscillation ν_{BO} (see, e.g., Strohmayer et al. 1996b). This was the main motivation for beat-frequency models such as the sonic-point model (Miller et al. 1998), which proposed that ν_u reflects the Keplerian frequency at the inner edge of the disk, and that ν_ℓ was the beat between ν_u and ν_s . As new observations revealed more sources showing both ν_{BO} and twin kHz QPOs, the relation became more complex (see Méndez & Belloni 2007 and van der Klis 2008 for a detailed historical overview). As a summary, NS-LMXBs are often classified as *fast* or *slow* rotators, depending on whether the spin frequency is higher or lower than ~ 400 Hz, respectively (Muno et al. 2001). It was found that generally the fast rotators follow $\Delta\nu \simeq \nu_s/2$, while slow rotators follow $\Delta\nu \simeq \nu_s$ (see Wijnands et al. 2003; Linares et al. 2005, and references therein). This of course implies that there is no one-to-one relation between the two quantities.

The question of whether $\Delta\nu$ and ν_s are physically related is still under debate. While current data might still be compatible with a bimodal rela-

¹At least in those source in which ν_{BO} was known. For example, $\Delta\nu$ in the neutron star LMXB Sco X-1 is known to vary (see, e.g. van der Klis et al. 1997).

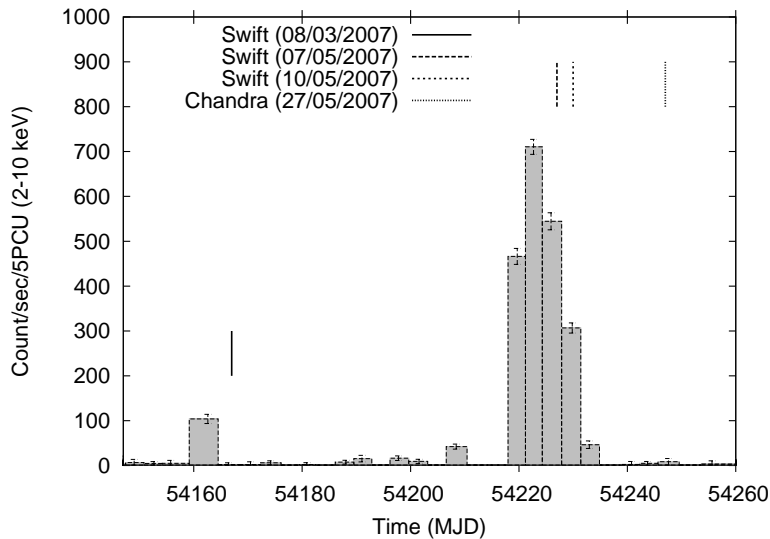


Figure 8.2: Light curve of IGR J17191-2821 as seen by the PCA bulge scan monitor program (Swank & Markwardt 2001). The times of the Swift and Chandra observations are marked with vertical lines.

tion, recent results suggest that this might not be the case. For example, Méndez & Belloni (2007) suggested that $\Delta\nu$ and ν_s are unrelated and that the division between fast and slow rotators may be just an effect of the low number of sources showing both phenomena (see also Yin et al. 2007). Recently, Strohmayer et al. (2008a) reported the discovery of burst oscillations at 414.7 Hz in the LMXB 4U 0614+091; if confirmed, these results would imply a spin frequency that is inconsistent with either $\Delta\nu \simeq \nu_s/2$ or $\Delta\nu \simeq \nu_s$ relations.

8.1.1 IGR J17191-2821

IGR J17191-2821 was discovered by the IBIS/ISGRI instrument aboard INTEGRAL during observations of the galactic bulge monitoring (Kuulkers et al. 2007b) conducted between the 2nd and the 4th of March, 2007 (Turler et al. 2007). The source was detected in the 20–40 and the 40–80 keV bands with significances of 10.4 and 4σ , and fluxes of 8.9 ± 0.9 and 5.8 ± 1.4 mCrab, respectively. The position of the source was first reported as (RA,DEC) = (259°.77, -28°.35) (J2000) with an accuracy of 2.5 arcmin.

On the 3rd of March 2007, RXTE Galactic bulge scans (Swank & Markwardt 2001) detected a source at a position consistent with that reported by Turler et al. (2007) at an intensity of 10 ± 1 mCrab in the 2-10 keV band (Swank et al. 2007). Three days later, a follow-up RXTE observation found the source at

flux levels of about 0.5 mCrab; a day later the source was not detected, with a 3σ upper limit of 1.2 mCrab. 8 years of Galactic bulge scans were reanalyzed for contributions from a source at the position of IGR J17191–2821, but no flares brighter than 2 mCrab were found. These non-detections showed that this source is active relatively infrequently (Swank et al. 2007).

During further Galactic bulge scan observations on April 29th and May 2nd of 2007, IGR J17191–2821 was detected again, but at a level of 30 and 70 mCrab (2–10 keV). This suggested that the previous detection was a flare or outburst precursor. Several Astronomical Telegrams at this time communicated on the discovery of Type I X-ray bursts (Klein-Wolt et al. 2007b; Markwardt et al. 2007a), burst oscillations (Markwardt et al. 2007a) and several episodes of kHz QPOs (Klein-Wolt et al. 2007c).

In this work, we present an intensive study of Type I X-ray burst characteristics, burst oscillations and kHz QPOs of this newly discovered neutron star LMXB IGR J17191–2821.

8.2 Observations and data analysis

8.2.1 Light curves, color diagrams and timing analysis

We use data from the Rossi X-ray Timing Explorer (RXTE) Proportional Counter Array (PCA; for instrument information see Zhang et al. 1993; Jahoda et al. 2006). To study the long-term (days/months) L_x behavior of the source, we used the PCA monitoring observations of the galactic bulge (Swank & Markwardt 2001). These observations are performed nine months of the year (as parts of the months of November, December, January and June are excluded due to solar constraints). The PCA bulge scans are capable of distinguishing a source position error of about 15 arcmin. The bulge scan light curves are given in the $\sim 2 - 10$ keV energy band.

To study the short-term (minutes or less) variability, we use PCA pointed observations. For IGR J17191–2821 there were 18 observations in one data set (92052-10) containing ~ 2.5 to ~ 10 ksec of useful data per observation. We use the 16-s time-resolution Standard 2 mode data to calculate X-ray colors. Hard and soft color are defined as the 9.7–16.0 keV / 6.0–9.7 keV and 3.5–6.0 keV / 2.0–3.5 keV count rate ratio, respectively, and intensity as the 2.0–16.0 keV count rate. Type I X-ray bursts were removed, background was subtracted and deadtime corrections were made. Colors and intensities were normalized by those of the Crab Nebula (see Kuulkers et al. 1994; van Straaten et al. 2003, see table 2 in Altamirano et al. 2008c for average colors of the Crab Nebula per PCU).

For the Fourier timing analysis we used the Event mode E_125us_64M_0.1s. Leahy-normalized power spectra were constructed using data segments of 128 seconds and 1/8192 s time bins such that the lowest available frequency is 1/128 Hz and the Nyquist frequency 4096 Hz. No background or deadtime corrections were performed prior to the calculation of the power spectra. Unless stated explicitly, in our fits we only include those Lorentzians whose single trial significance exceeds 3σ based on the error in the power integrated from 0 to ∞ . For the kHz QPOs, we report the centroid frequency ν_0 , the full width at half maximum (FWHM) and the rms amplitude. The quoted errors use $\Delta\chi^2 = 1.0$. The upper limits quoted in this paper correspond to a 95% confidence level ($\Delta\chi^2 = 2.7$).

8.2.2 Energy spectra of the persistent emission

For the PCA, we used the Standard 2 data of PCU 2, which was active in all observations. The background was estimated using the PCABACKEST version 6.0 (see FTOOLS). We calculated the PCU 2 response matrix for each observation using the FTOOLS routine PCARSP V10.1. For the HEXTE instrument, spectra were accumulated for cluster B (as cluster A stopped rocking in October 2006), excluding the damaged detector and averaging both rocking directions to measure the background spectrum. Dead time corrections of both source and background spectra were performed using HXTDEAD V6.0. The response matrices were created using HXTRSP V3.1. For both PCA and HEXTE, we filtered out data recorded during, and up to 30 minutes after passage through the South Atlantic Anomaly (SAA). We only used data when the pointing offset from the source was less than 0.02 degrees and the elevation of the source respect to the Earth was greater than 10 degrees. Using XSPEC V11.3.2i (Arnaud 1996), we fitted simultaneously the PCA and HEXTE energy spectra using the 3.0–25.0 keV and 20.0–200.0 keV energy bands, respectively. We used a model consisting of a disk blackbody and a power law, absorbed with an equivalent Hydrogen column density of $0.3 \times 10^{22} \text{ cm}^{-2}$ (Klein-Wolt et al. 2007a), which gave a good fit in all the observations ($\chi^2/dof < 1.1$).

8.2.3 Type I X-ray bursts

We searched the Standard 1 mode data (2–60 keV, 0.125 seconds time resolution, no energy resolution) of the 18 observations. We found 5 Type I X-ray bursts (see Table 8.1).

We searched each burst for coherent pulsations using the Z_n^2 statistic (Strohmayer & Markwardt 1999). We computed Z_1^2 (i.e. assuming that the

signal is sinusoidal) throughout the bursts using a sliding 2 seconds window with a step of 0.125 sec. The Z_1^2 statistic has the same statistical properties as a Leahy normalized power spectrum, which means that for a purely random Poisson process, the powers follow a χ^2 distribution with 2 degrees of freedom (Strohmayer & Markwardt 1999). We searched the 30–4000 Hz frequency range in the 2–60 keV band and in narrower energy bands (Sec. 8.3.2).

We also created energy spectra every 0.25 sec from the Event mode (E_125us_64M_0_1s) data of all the PCUs that were on during the burst. Given the high count rates during the peak of the bursts, we corrected each energy spectrum for dead-time using the methods suggested by the RXTE team². For each energy spectrum, we created the corresponding response matrix using the latest information available on the response of the instrument at the relevant times. As is common practice, we used as background the energy spectrum of the persistent emission taken seconds before each burst. (We used 100 sec of the persistent emission to calculate the spectrum. However, we found no significant differences in the fits when the persistent-emission before or after the burst was used, or when using data-segments of different lengths -between 100 and 500 seconds-). We used a black-body model to fit the resulting burst spectra³.

8.3 Results

8.3.1 Position of the source

Swift observed the source twice on March 8th 2007 (at 02:37 UT for a total of ~ 800 sec, and at 10:44 UT for a total of ~ 1600 sec – both observations were performed in in PC mode). These are the only Swift observations performed

²http://heasarc.gsfc.nasa.gov/docs/xte/recipes/pca_deadtime.html

³We assumed that the X-ray spectra after the persistent emission has been subtracted are Planckian and that the observed luminosity of the source is:

$$L = 4\pi\sigma T^4 R^2,$$

so the unabsorbed bolometric X-ray flux may be determined using

$$F_{bol} = \sigma T^4 (R/D)^2,$$

where σ is the Stefan-Boltzmann constant, T is the black-body temperature, R the neutron star photosphere radius, and D the distance to the source. The ratio $(R/D)^2$ is the normalization of the black-body model we used (*bbodyrad* – see Xspec manual for details). We note that X-ray burst spectra are generally well described by black-body emission, however, the emission from the neutron star and its environment (e.g. accretion disk) is expected to be more complex than simple black-body emission (see, e.g., van Paradijs 1982; London et al. 1984; Kuulkers et al. 2003, and references therein).

before the bright outburst (see Section 8.3.4). The observations were taken in Photon Counting mode and did not show a source *within* the INTEGRAL error circle with an upper limit of $0.0021 \text{ cnts s}^{-1}$ (at a 95% confidence level). Assuming a galactic absorption of $3.4 \times 10^{21} \text{ cm}^{-2}$ and a photon index of 1.8, this countrate translates into an upper limit of $\sim 8.7 \times 10^{-14} \text{ erg s}^{-1} \text{ cm}^{-2}$ on the unabsorbed flux (approximately 0.004 mCrab in the 2-10 keV range). We found a source in the first Swift observation (i.e. on March 8th at 2:37 UT) located at a distance of about 3.5 arcminutes from the INTEGRAL position. Its coordinates are (RA, DEC) = (259.8114, -28.3005) (J2000), with an error of ~ 9 arcsec. We measured an average count rate of $0.0087 \text{ cnts s}^{-1}$, which corresponds to an unabsorbed flux of $3.6 \times 10^{-13} \text{ erg s}^{-1} \text{ cm}^{-2}$ or 0.02mCrab (2-10 keV, assuming the same N_h and photon index as above). In the second Swift observation this source is not significantly detected (a total of three photons within a 10 pixel source error circle and zero from a background region 3 times as large). We place a 95% confidence upper limit on the 2-10 keV unabsorbed flux of $\sim 2.0 \times 10^{-13} \text{ erg s}^{-1} \text{ cm}^{-2}$ (employing PIMMS⁴ for an absorbed power-law spectrum with $N_h = 3.4 \times 10^{21} \text{ cm}^{-2}$ and a photon index of 1.8, and applying the prescription for low number statistics given by Gehrels 1986). In Figure 8.1 we show the Swift/XRT images of the region around the source for the 2 observations on March 8th (upper panels). For comparison, in the lower panels we show the Swift/XRT images of two observations during IGR J17191–2821 outburst (May 7th and 10th, 2007).

As noted by Klein-Wolt et al. (2007a), the formal INTEGRAL error circle on the position of IGR J17191–2821 would suggest that the faint source we detected with Swift is unrelated to IGR J17191–2821 (its position is 1 arcminute outside the INTEGRAL error circle for the position of IGR J17191–2821, see Figure 8.1). However, given the systematic uncertainties in the INTEGRAL position, both sources are probably one and the same. We note that this is not the first case in which the true position of a transient laid outside the reported INTEGRAL-IBIS/ISGRI error circle (see e.g. Kuulkers et al. 2007a).

8.3.2 Thermonuclear X-ray bursts and the distance to the source

We found 5 Type I X-ray bursts (see Table 8.1). All bursts showed similar temperature, radius and bolometric flux profiles (not shown). The temperature and flux profiles were all single peaked, and reached their maxima within a second. The maximum temperature (kT) was always between 2 and 3 keV and the peak bolometric fluxes were in the $2-3 \times 10^{-8} \text{ erg s}^{-1} \text{ cm}^{-2}$ range (Ta-

⁴<http://heasarc.gsfc.nasa.gov/Tools/w3pimms.html>.

ble 8.1). In all cases, the black-body radius remained approximately constant after the peak and was usually constrained between 5 and 10 km (assuming a distance of 11 kpc). None of the bursts showed indications of photospheric radius expansion. By using the highest measured bolometric peak flux of $3 \times 10^{-8} \text{ erg s}^{-1} \text{ cm}^{-2}$ we can estimate an upper limit on the distance. We find a distance $D < 11 \text{ kpc}$ when using the empirically determined Eddington luminosity of $3.79 \times 10^{38} \text{ erg s}^{-1}$ (for bursts showing photospheric radius expansion – Kuulkers et al. 2003). Using a more complex approximation⁵ and standard values for the mass and the radius of the neutron star (i.e. $M_{NS} = 1.4M_{\odot}$ and $R = 10 \text{ km}$), we found $D < 8.6$ and $D < 6.6$ for hydrogen mass fractions of $X = 0$ and $X = 0.7$, respectively. Higher values of R give higher upper limits.

Table 8.1: X-ray bursts in IGR J17191–2821.

Number	ObsID (92052-10)	Start time of the burst (UT, 2007)	Num. of PCUs on	Flux ^a (10^{-8} $\text{erg s}^{-1} \text{ cm}^{-2}$)	Osc. (yes/no)	Osc. rms amplitude ^b (2–17 keV)
1	-01-00	May 4 02:32:06	2	2.5 ± 0.3	yes	$6.9 \pm 0.6\%$
2	-05-00	May 7 02:39:39	2	2.9 ± 0.3	yes	$5.0 \pm 1.0\%$
3	-03-01	May 7 05:51:12	2	2.7 ± 0.3	no	< 3%
4	-06-00	May 8 17:08:53	3	2.6 ± 0.2	yes	$10.2 \pm 1.5\%$
5	-06-01	May 8 20:38:44	2	2.1 ± 0.3	no	< 3%

^a:Bolometric peak flux.

^b:Integrated amplitude of the oscillations in the 2–17 keV range.

8.3.3 kHz QPOs

We searched the averaged power spectrum of each observation for the presence of significant kHz QPOs at frequencies $\gtrsim 200 \text{ Hz}$. In each case, we fitted the power spectra between 200 and 4000 Hz with a model consisting of one or two Lorentzians and a constant to account for the presence of QPOs and Poisson noise, respectively. We found that 12 out of the 17 observations show significant QPOs in the 605–1185 frequency range. In 4 observations we detected 2

⁵The approximation was recently used by Galloway et al. (2008b) to compare a sample of more than a thousand X-ray burst from different sources. The distance is given by:

$$D = 8.6 \cdot \left(\frac{Flux_{Bol}}{3 \cdot 10^{-8} \text{ erg cm}^{-2} \text{ s}^{-1}} \right)^{-1/2} \cdot \left(\frac{M_{NS}}{1.4M_{\odot}} \right)^{1/2} \cdot \left(\frac{1+z(R)}{1.31} \right)^{-1/2} \cdot (1+X)^{-1/2} \text{ kpc}$$

where M_{NS} is the mass of the neutron star in solar masses, X is the mass fraction of hydrogen in the neutron star atmosphere and $z(R)$ is the term that takes into account the gravitational redshift at the photosphere (were $1+z(R) = (1-2GM_{NS}/Rc^2)^{-1/2}$, G is the gravitational constant, c the speed of light and R the radius measured at the photosphere – see Galloway et al. 2008b).

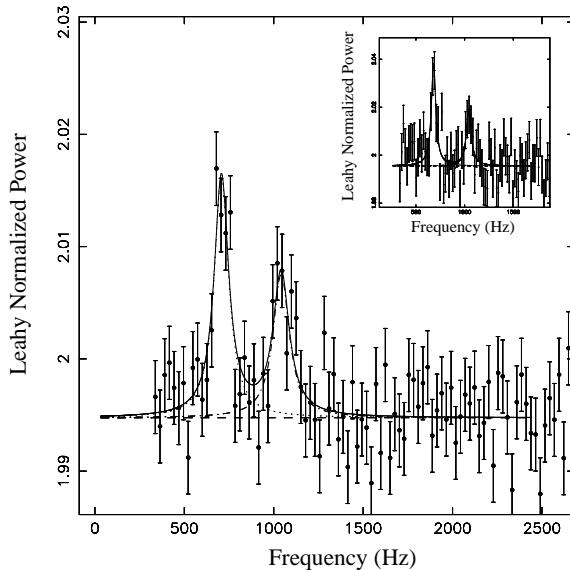


Figure 8.3: kHz QPOs after the shift-and-add. The lower kHz QPO was shifted to the arbitrary frequency of 700 Hz (see Section 8.3.3). Inset: kHz QPOs in observation 92052-10-05-00. See also Table 8.2.

simultaneous kHz QPOs (see Table 8.2). The lower kHz QPO frequency was between 680 and 870 Hz, with single trial significance between 5.7 and 10σ . The upper kHz QPO frequency was between 1037 and 1085 Hz, with single trial significances between 3.0 and 3.7σ . $\Delta\nu$ showed no significant changes and was always consistent with 350 Hz (see Table 8.2).

We tried to better constrain $\Delta\nu$ by using the shift-and-add method as described by Mendez et al. (1998b). We first tried to trace the detected kilohertz QPO using a dynamical power spectrum (e.g. see figure 2 in Berger et al. 1996) to visualize the time evolution of the QPO frequency, but the signal was too weak to be detected on timescales shorter than the averaged observation. Therefore, for each observation we used the fitted averaged frequency to shift each lower kHz QPO to the arbitrary frequency of 700 Hz. Next, the shifted, aligned, power spectra were averaged. The average power spectrum was finally fitted in the range 300–2048 Hz so as to exclude the edges, which are distorted due to the shifting method. To fit the averaged power spectrum, we used a function consisting of two Lorentzians and a constant to fit the QPO and the Poisson noise, respectively. In this case, the averaged $\Delta\nu$ is 332 ± 16 Hz. In Figure 8.3 we show the shift-and-added power spectrum and a representative example of the single observation power spectrum with two kHz QPOs (see inset).

Table 8.2: Observations and kHz QPOs.

ObsID (92052-10)	MJD (days)	Aver. Cts/s ^a /PCU2	PCUs on ^b	Lower kHz QPO			Upper kHz QPO			$\Delta\nu$ (Hz)
				ν (Hz)	FWHM (Hz)	rms (%)	ν (Hz)	FWHM (Hz)	rms (%)	
-01-00	54224.09	182	2	–	–	–	–	–	–	–
-02-00	54225.07	170	3-4	870 ± 1	11 ± 1.7	8.5 ± 0.4	1185 ± 50	220 ± 94	9.2 ± 1.5	315 ± 50
-02-01	54225.14	188	3	866 ± 3	38 ± 6	9.2 ± 0.6	–	–	–	–
-03-00	54226.21	172	1-3	881 ± 10	132 ± 23	15 ± 1	–	–	–	–
-05-00	54227.10	142	2-3	681 ± 5	55.2 ± 15	10.3 ± 0.9	1043 ± 10	60 ⁺²⁷ ₋₁₉	8.4 ± 1.1	362 ± 11
-03-01	54227.23	148	2	730 ± 1	13.2 ± 2.7	9.7 ± 0.6	1075 ± 12	55 ⁺³² ₋₂₂	8.5 ± 1.3	345 ± 12
-04-00	54228.01	156	3	891 ± 3	37.7 ± 7.5	9.4 ± 0.6	–	–	–	–
-04-01	54228.20	151	2-3	838 ± 1	25 ± 4	9.3 ± 0.4	–	–	–	–
-06-00	54228.70	129	2-3	946 ± 20	151 ⁺⁶⁶ ₋₄₁	10.6 ± 1.2	–	–	–	–
-06-01	54228.90	130	2-3	702 ± 3	37 ± 7	10.4 ± 0.6	1037 ± 15	88 ⁺⁴³ ₋₂₇	8.8 ± 1.1	335 ± 15
-07-00	54229.06	105	1-2	884 ± 13	108 ⁺⁵³ ₋₃₁	15 ± 2	–	–	–	–
-07-01	54229.98	72	2	706 ± 10	83 ± 25	18 ± 2	–	–	–	–
-05-01	54230.04	70	2	682 ± 20	172 ⁺⁷⁸ ₋₅₅	22.4 ± 2.8	–	–	–	–
-08-00	54231.09	46	2	–	–	–	–	–	–	–
-08-01	54231.75	27	2-3	–	–	–	–	–	–	–
-09-00	54232.01	23	3	–	–	–	–	–	–	–
-09-01	54232.08	21	3-4	–	–	–	–	–	–	–

^a: Background and deadtime corrected averaged count rate for PCU2; this PCU was on during all observations.

^b: In case the number of active PCUs changed, we report the minimum and maximum number.

8.3.4 Outburst evolution

Figure 8.2 shows the PCA light curve of IGR J17191–2821 as seen by the PCA bulge scan monitor program (Swank & Markwardt 2001). While a precursor of the outburst (see Section 8.1.1) occurred at MJD 54162.6, the full X-ray outburst did not start until 54 days later (i.e. MJD 54216); it lasted for about 30 days.

On MJD 54247 (May 27th, 2007) the source was not detected anymore with RXTE, and a Chandra/HRC-I observation was performed. As reported by Chakrabarty et al. (2007), the source was not detected in the 1.1 ks observation within the 30 arcsec of the Swift/XRT position (see Section 8.3.1). These authors estimated an upper limit on the 0.3–10 keV unabsorbed flux of $< 8.3 \times 10^{-14} \text{ erg s}^{-1} \text{ cm}^{-2}$.

In Figure 8.4 we show the persistent unabsorbed 2–200 keV flux (panel *a*), power law index (panel *b*), strength of the broad band noise (panel *c*) and kHz QPO frequency (panel *d*) as a function of time during the ~ 3 weeks of the outburst from which RXTE pointed observations are available. The source reached a maximum flux of $\sim 2.5 \times 10^{-9} \text{ erg cm}^2 \text{ s}^{-1}$. Assuming $D < 11 \text{ kpc}$ (see Section 8.3.2), we place an upper limit on the outburst peak luminosity of $4 \times 10^{37} \text{ erg s}^{-1}$. In panel *a* of Figure 8.4 we also plot the (Type I) X-ray burst bolometric peak fluxes at the time they occurred (as detected by RXTE).

Due to the relatively low count rates collected by the PCA, the average power spectrum of each observation had low statistical quality. However, in the brightest (and softest) observations we found traces of the so-called very low frequency noise (VLFN). A steep power-law rised below 1 Hz towards the lowest frequencies, this VLFN is a typical signature of the so called “banana branch” (soft state) of atoll sources (see, e.g., van der Klis 2006, for a review). When comparing the results showed in the different panels of Figure 8.4, we found that the 5–50 Hz averaged fractional rms amplitude is anti-correlated with the source luminosity, whereas the frequencies of both kHz QPOs showed no obvious trend. The spectral index was clearly anti-correlated with the strength of the variability (i.e, correlates with luminosity). This is similar to what has been found in other atoll sources (see, e.g., van der Klis 2006, for a review), where the strength of the variability and the spectral index trace the changes in the timing and spectral state during the outburst. By studying the time evolution of these two quantities (Fig. 8.4) we found that the source was initially in the soft (banana) state and showed a failed transition to the hard (extreme island) state around MJD 54226. After this, it re-brightened and returned to the soft state. On MJD 54228 (i.e. two days later) the luminosity reached a secondary peak and started to decline, while the source gradually transitioned from the soft (banana) state to the hard (extreme island) state.

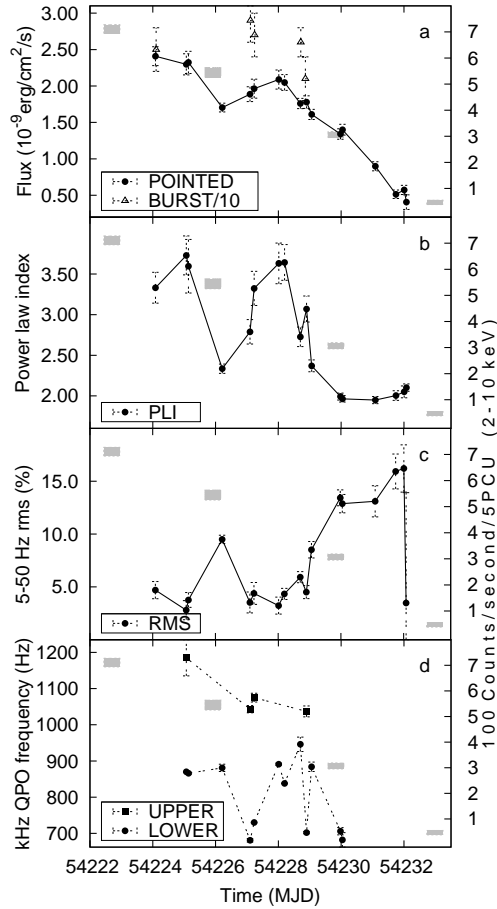


Figure 8.4: Spectral and timing properties along the outburst of IGR J17191–2821. From top to bottom, *a*): 2–200 keV unabsorbed persistent flux (filled circles) and bolometric peak flux of the type I X-ray bursts detected by the PCA (open triangles; flux values are divided by ten for plotting purposes); *b*): power law index obtained from the broad band spectral fits; *c*): fractional rms amplitude of the variability between 5 and 50 Hz in the ~ 2.5 –45 keV energy band and *d*): frequencies of the upper (squares) and lower (circles) kHz QPOs detected during the outburst. The grey rectangles show the flux measured by the PCA Galactic bulge scans (right axis; see also Figure 8.2).

Finally IGR J17191–2821 faded below the detection limit of RXTE-PCA. The timing and spectral properties (and evolution) allow us to firmly establish the atoll source nature of IGR J17191–2821.

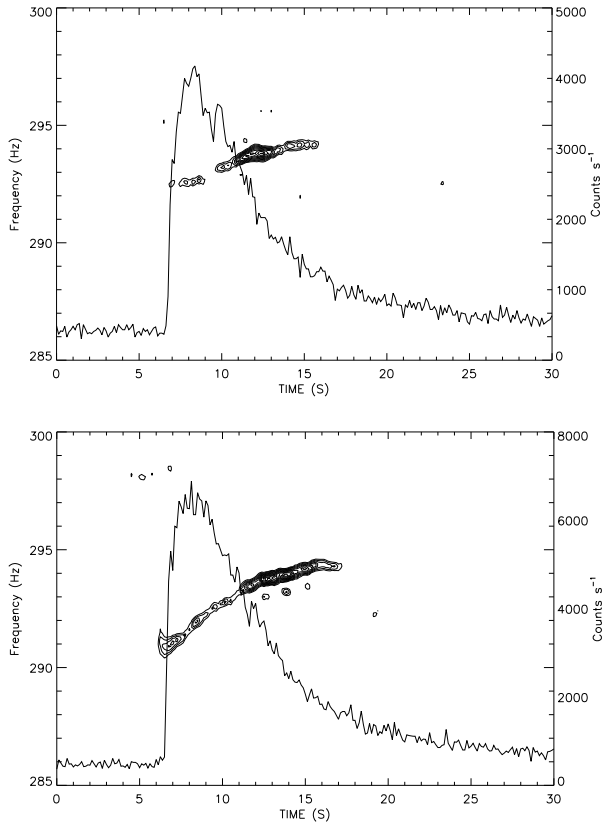


Figure 8.5: Lightcurve and dynamical power spectra (2–60 keV) for bursts 1 and 4 (upper and lower panel, respectively – see also Table 8.1). The dynamical power spectra were created using overlapping 2 s windows, with new windows starting at 0.125 s intervals. We used a Nyquist frequency of 4096 Hz. The contours show Leahy normalized powers between 20 and 60, increasing in steps of 5.

8.3.5 Burst oscillations

By applying the Z_1^2 method (see Section 8.2.3) on the 2–60 keV X-ray burst data, we discovered highly significant nearly-coherent oscillations in 2 of the 5 X-ray bursts (Burst 1 and 4 in Table 8.1). For the remaining 3 bursts, we repeated the Z_1^2 analysis using only data in different energy sub-bands. We found that the oscillations were significantly detected also in burst number 2, but only in the 10–25 keV range. The oscillations are not significantly detected in either burst 3 or 5. Fractional rms amplitudes (averaged over the period the signal was significantly detected) and upper limits are given in Table 8.1. In Figure 8.5 we show the dynamical power spectra of bursts 1 and

4 (upper and lower panels, respectively) in the 2–60 keV range. Maximum Z_1^2 powers of ~ 63 were found in both cases. As can be seen, the frequency of these oscillations increases with time as usually seen for burst oscillations during Type I X-ray bursts (see, e.g., Strohmayer 2001, for a review). During bursts 1 and 4, the frequency drifts from ~ 291 Hz and ~ 292.5 Hz, respectively, until it reaches a frequency between 294 and 294.5 Hz.

8.3.6 The energy dependence of the burst oscillations

We analyzed the energy dependence of bursts 1 and 4 which showed the strongest oscillations – see Table 8.1. We split the data in six energy bands (from 2.5 keV to 17 keV), and calculated the amplitude of the pulsations in each band. To create a pulse profile in each energy band, we selected all the data with a significant pulse detection in the corresponding power spectrum, and explored the $P - \dot{P} - \ddot{P}$ space around a given initial guess value for the pulse period (obtained from the power spectrum). \dot{P} and \ddot{P} were initially set to zero. We note that \dot{P} and \ddot{P} do not represent true spin changes of the neutron star, but comprise all the frequency variations due, primarily, to the burst oscillation drift seen in the data. \dot{P} and \ddot{P} are therefore useful to align the phases of the pulsations (folded in a profile of 32 bins) for each energy band. We then fitted the pulse profiles with two sinusoids representing the fundamental and the 1st overtone of the burst oscillations. The errors on the fractional amplitudes are calculated using a $\Delta\chi^2 = 1$. Upper limits are at a 95% confidence level (i.e. using $\Delta\chi^2 = 2.7$). We found no significant second harmonic in any of the energy bands we chose for either burst, with rms amplitude upper limits in the 2.5 – 17 keV range of 3.7% and 2.0% for bursts 1 and 4, respectively. The energy dependence of the burst oscillation rms amplitude is shown in Figure 8.6. The fractional amplitude of the fundamental increases slightly with energy; a possible dip in the 5–7 keV band is seen in both bursts. No significant phase lags were detected.

8.4 Discussion

The energy and broadband power spectra of IGR J17191–2821 evolved in a manner consistent with that seen in other neutron star LMXBs: the source is soft when the flux is high and hard when the flux is low, and near the end of the outburst it shows the hardest spectra and strongest variability, with an rms amplitude above 15%. We detected thermonuclear X-ray bursts, some of them showing burst oscillations at $\nu_{BO} \sim 294$ Hz. This ν_{BO} is within the range observed in other sources (i.e. 45–619 Hz, see, e.g. Watts et al. 2008a,

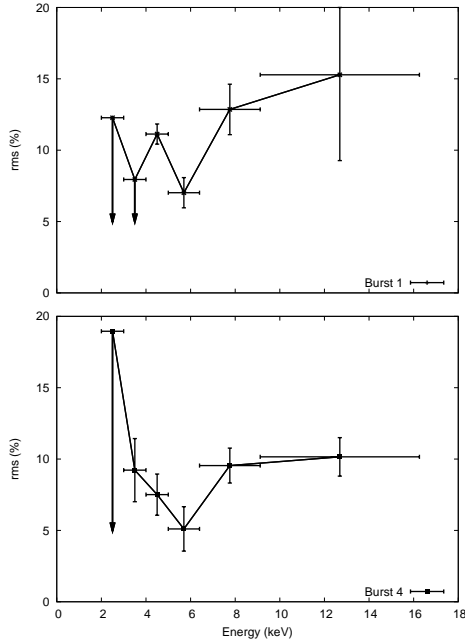


Figure 8.6: Fractional rms amplitude versus energy for the oscillations in X-ray bursts 1 and 4 (See Table 8.1). Arrows mark upper limits at 95% confidence level.

and references within). The energy dependence of the burst oscillations is consistent with a slight increase at higher energies. This is similar to what has been found for burst oscillations in other NS systems (see, e.g., Munro et al. 2003). We also detected several episodes of kHz QPOs. When two were detected simultaneously, the difference in frequency was approximately constant (See Table 8.2). These results allow us to firmly establish the atoll source nature of IGR J17191–2821.

Two months before the main outburst, the source exhibited a very brief (only days) event which was nearly an order of magnitude less luminous. It is unclear what the relation of this event is with respect to the main outburst. However, we note that similar precursors have been seen before (see, e.g., Degenaar & Wijnands 2009). To our knowledge, no systematic search has been performed in order to quantify how common these precursors are and how they can be explained in the commonly used disk-instability models proposed for outbursts of X-ray binaries (see Lasota 2001, for a review).

There are presently 12 LMXBs with reported measurements of $\Delta\nu$ whose spin can be estimated from either burst oscillations or from pulsations in their persistent X-ray emission (van der Klis 2008, for a recent overview). In

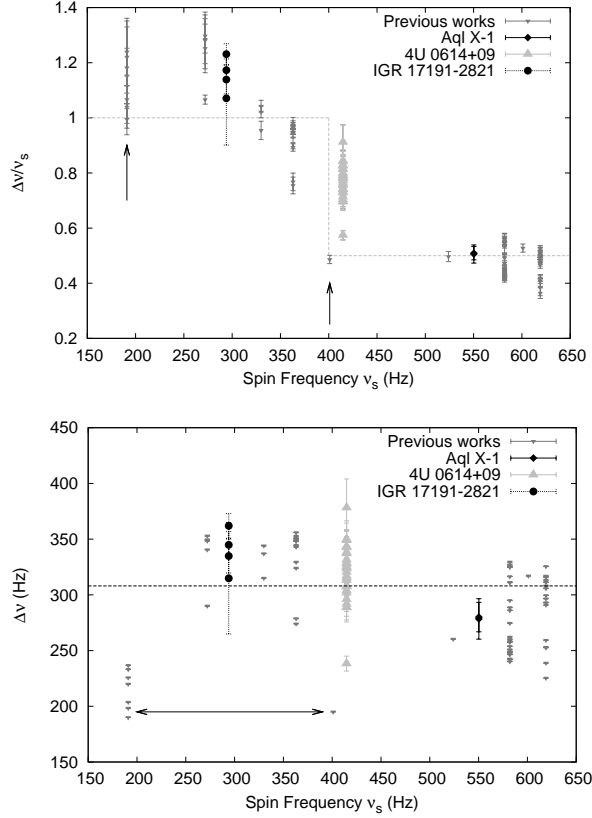


Figure 8.7: In the upper panel we plot the ratio between the individual measurements of $\Delta\nu = \nu_u - \nu_\ell$ and the spin frequency ν_s as a function of ν_s (cf. van der Klis 2006; Méndez & Belloni 2007; van der Klis 2008). Spin frequencies are as estimated from the persistent pulsations observed in AMXPs (marked with the arrows) or from burst oscillations in the non-pulsating sources. The dashed line shows the step function $S(\nu_s) = 1$ for $\nu_s \leq 400$ Hz; $S(\nu_s) = 0.5$ for $\nu_s > 400$ Hz. The lower panel shows the same data as above. The horizontal dashed line corresponds to a constant $\Delta\nu = 308$ Hz (Méndez & Belloni 2007). For 4U 0614+09 we used the tentative burst oscillation frequency of 414.7 Hz (Strohmayer et al. 2008a) and the kHz QPOs measurements reported by van Straaten et al. (2000). For Aql X-1 we used $\nu_s = 550$ Hz (e.g. Casella et al. 2008, and references within) and the tentative $\Delta\nu$ measurements reported by Barret et al. (2008). IGR J17191–2821 data are from this work.

Figure 8.7 (upper panel) we plot $\Delta\nu/\nu_s$ vs. ν_s for all these sources (cf. van der Klis 2006; Méndez & Belloni 2007; van der Klis 2008). The dashed line represents a step function: $\Delta\nu/\nu_s \sim 1$ for the slow rotators (< 400 Hz) and $\Delta\nu/\nu_s \sim 0.5$ for the fast rotators (> 400 Hz). Although most of the data seems to be consistent with this scheme (and our data of IGR J17191–2821

are as well), certainly there are points that do not follow this relation. A clear example is given by the neutron star 4U 0614+09. A tentative ~ 414.7 Hz burst oscillation frequency was recently reported for this source (Strohmayer et al. 2008a, note that we quote this value as tentative given that it has been detected only once, the signal showed no frequency drift as expected from burst oscillations, and it was the first and only detection to date of burst oscillations with the Burst Alert Telescope on board the Swift telescope). As shown in Figure 8.7 this burst oscillation frequency is very close to the discontinuity of the step function (although given the present data, the discontinuity of the step function could be anywhere between ~ 360 and 401 Hz). At the same time, $\Delta\nu/\nu_s$ covers almost the complete 0.5-1 range (van Straaten et al. 2000; Boutelier et al. 2008).

Méndez & Belloni (2007) have recently suggested that $\Delta\nu$ and ν_s are unrelated and that the division between fast and slow rotators may be just an effect of the low number of sources showing both phenomena (see also Yin et al. 2007). In the lower panel of Figure 8.7 we show $\Delta\nu$ and ν_s for the same data plotted in the upper panel. The dashed line in this panel corresponds to the average $\Delta\nu = 308$ Hz suggested by Méndez & Belloni (2007). As can be seen, the $\Delta\nu$ range of most sources overlaps with this constant value, except for the two AMXPs SAX J1808.4–3658 and XTE J1807–294, for which $\Delta\nu$ falls clearly below 300 Hz. The discrepancy is solved, if the data for these two sources are multiplied by a factor of 1.5. This was first suggested by Méndez & Belloni (2007) based on the works of van Straaten et al. (2005) and Linares et al. (2005)⁶. We note that not all AMXPs are affected by the same multiplicative factor (van Straaten et al. 2005), and furthermore, that the factor might be independent of whether the neutron star pulsates or not (Altamirano et al. 2005).

Clearly, the present data are not enough to draw any final conclusions, so the detection of ν_s , ν_{BO} and $\Delta\nu$ in other sources is necessary. The new instrument ASTROSAT (an Indian multiwavelength Astronomy Satellite), which is planned to be launched in 2010, will play a major role, as it is likely to increase the sample of sources with both spin frequency and kHz QPOs measurements.

⁶Previous works have shown that the frequencies of the variability components observed in atoll sources follow a universal scheme of correlations when plotted versus ν_u (see e.g. van Straaten et al. 2002, 2003; Reig et al. 2004; Altamirano et al. 2008c, and references therein). The two AMXPs SAX J1808.4–3658 and XTE J1807–294 show similar relations. However, the relations for these two sources are shifted with respect to those of the other sources (van Straaten et al. 2005; Linares et al. 2005). This shift is between the frequencies of the low-frequency components and ν_u by a factor around 1.5 (1.45 and 1.59 for SAX J1808.4–3658 and XTE J1807–294, respectively) and between ν_ℓ and ν_u by a similar factor.